

## Supplementary material

### Reconstructive Phase Transition in Ultrashort Peptide Nanostructures and Induced Visible Photoluminescence

Amir Handelman<sup>1\*</sup>, Natalia Kuritz<sup>2</sup>, Amir Natan<sup>2</sup> and Gil Rosenman<sup>2\*</sup>

<sup>1</sup>Department of Electrical Engineering, Faculty of Engineering, Holon Institute of Technology, 52 Golumb st. Holon, Israel.

\*Correspondence to Amir Handelman; [handelmana@hit.ac.il](mailto:handelmana@hit.ac.il)

<sup>2</sup>School of Electrical Engineering-Physical Electronics, Faculty of Engineering, Tel Aviv University, Ramat Aviv, 69978 Tel Aviv.

\*Correspondence to Gil Rosenman; [rgil@post.tau.ac.il](mailto:rgil@post.tau.ac.il)

#### 1. Molecular Structure

The molecular structures of the studied in this paper di- and tripeptides are illustrated in Figure 1.

- a. linear aromatic FF dipeptide ( $\text{NH}_2\text{-L-Phe-L-Phe-COOH}$ , formula:  $\text{C}_{18}\text{H}_{20}\text{N}_2\text{O}_3$ , Relative Molecular Mass: 313).
- b. linear LL dipeptide ( $\text{NH}_2\text{-L-Leu-L-Leu-COOH}$ , formula:  $\text{C}_{12}\text{H}_{24}\text{N}_2\text{O}_3$ , Relative Molecular Mass: 245).
- c. linear FFF tripeptide ( $\text{NH}_2\text{-L-Phe-L-Phe-L-Phe-COOH}$ , formula:  $\text{C}_{27}\text{H}_{29}\text{N}_3\text{O}_4$ , Relative Molecular Mass: 460).
- d. cyclic FF tripeptide (Cyclo(-Phe-Phe), formula:  $\text{C}_{18}\text{H}_{18}\text{N}_2\text{O}_2$ , Relative Molecular Mass: 295).

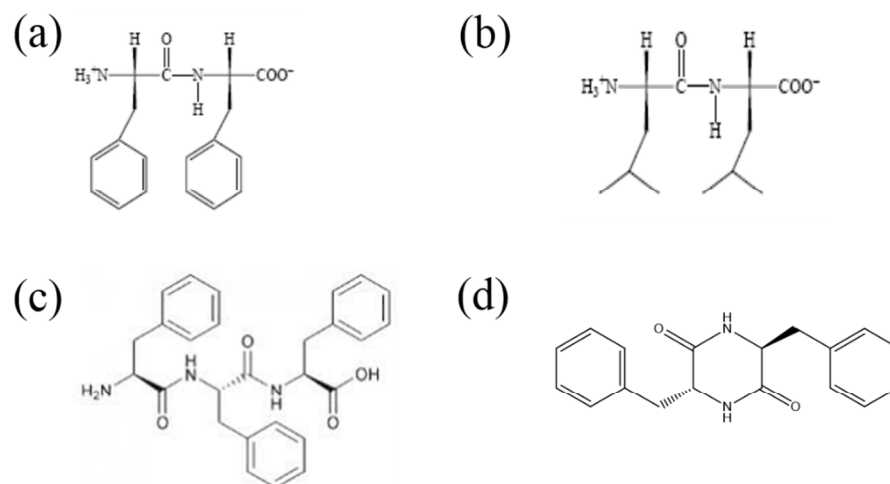


**Figure 1.** Molecular structure of: (a) linear FF dipeptide, (b) linear LL dipeptide, (c) linear FFF dipeptide, and (d) Cyclo-FF dipeptide.

## 2. Fourier transform infrared spectroscopy (FTIR): experimental data and discussion.

To examine the peptide secondary structure of the studied in this paper di- and tripeptides in their native and thermally-induced phases two methods of Circular Dichroism (CD)<sup>1</sup> and Fourier transform infrared spectroscopy (FTIR)<sup>2</sup> were applied. CD and FTIR are the standard methods for recognition of biological secondary structures such as  $\beta$ -sheet structures.

CD data are described in details in the main text of the paper. We showed that despite native FF-, LL- and FFF- nano-architectures are self-assembled by dissimilar intramolecular interactions, all these nanostructures are re-folded at elevated temperature into similar amyloid-like fibrous morphology having the same antiparallel extended  $\beta$ -sheet secondary structure. Cyc-FF nanofibers assembled from original Cyc-FF show

amazing stability and stays in its native morphology and secondary structure until 200C which was attributed to a  $\beta$ -turn or  $\alpha$ -helix<sup>3</sup>.

This assumption is supported by Fourier Transform Infrared (FTIR) analysis. The FTIR spectra were studied in the most sensitive spectral region of peptide/protein secondary structures at the wavelengths 1600-1700  $\text{cm}^{-1}$  related to the amide I vibrational band<sup>4</sup> (Figure 2).

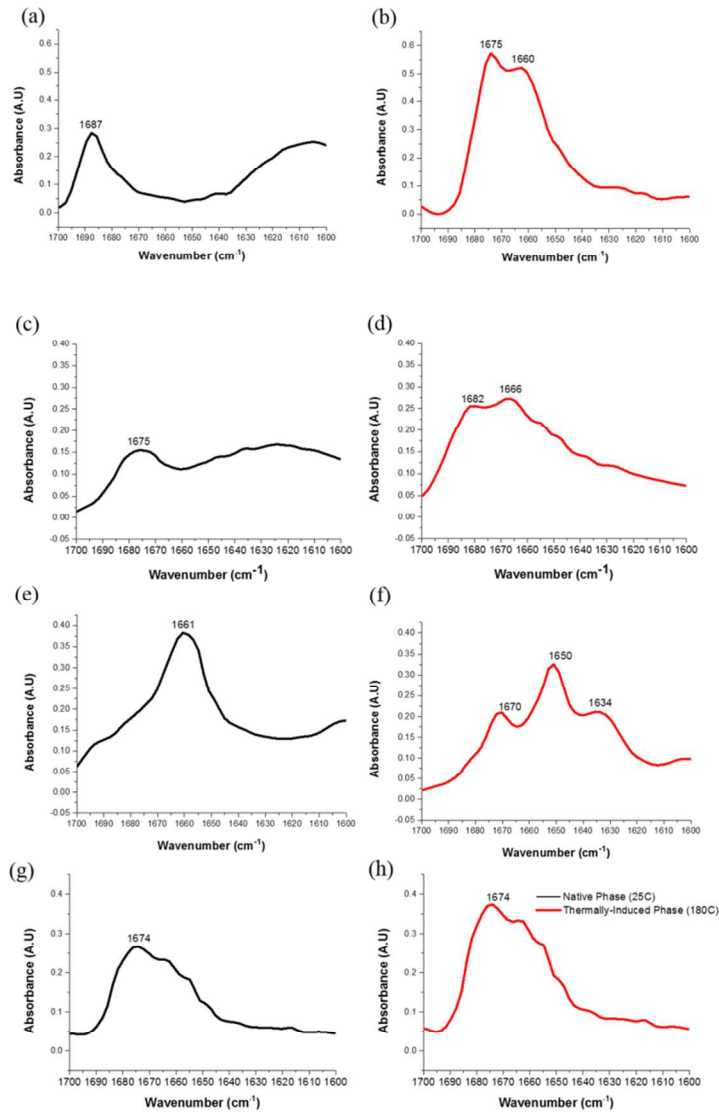


**Figure 2.** FTIR spectra in the native phase (black) of (a) FF PNT, (c) LL PNT, (e) FFF nano-spheres and (g) originally Cyc-FF PNF, and in the thermally-induced phase (red) of (b) FF PNF, (d) LL PNF, (f) FFF PNF, and (h) thermally treated Cyc-FF PNF.

In the native phase FF nanotubes demonstrate a single peak at  $1687\text{ cm}^{-1}$  (Figure 2, a) related to the C=O vibration modes of the amide I region<sup>4</sup>. According to the previous works<sup>4,5,6</sup> this peak can be assigned to a  $\beta$ -turn secondary structure with contribution from a minor  $\beta$ -sheet conformation<sup>7,8</sup>. This FTIR peak was observed in other study of FF nanotubes<sup>6</sup>.

In the thermally-induced phase (Figure 2, b), the FTIR spectrum of FF -fibers is strongly modified. The single peak of the native phase peak vanishes and two new peaks in the same amide I region appear:  $1660\text{ cm}^{-1}$  and  $1675\text{ cm}^{-1}$ . While the first peak, at  $1660\text{ cm}^{-1}$  shows a slight tendency to  $\beta$ -turn secondary structure<sup>7,8</sup>, the  $1675\text{ cm}^{-1}$  peak is attributed to  $\beta$ -sheet conformation<sup>4,9,10</sup>. Similar behavior of splitting peaks related to the C=O vibration modes during thermal treatment of LL nanotubes (Figure 2, d) and FFF nanospheres (Figure 2, f).

Before heating, in the native phase of the LL nanotubes, a sharp peak at  $1675\text{ cm}^{-1}$  and a wide peak at  $1623\text{ cm}^{-1}$ , both in the amide I region are observed (Figure 2 c). The peak at  $1675\text{ cm}^{-1}$  was already mentioned above and can be related to either  $\beta$ -turn or  $\beta$ -sheet secondary structure, while the wide peak at  $1623\text{ cm}^{-1}$  indicates that the LL nanotubes also have a  $\beta$ -sheet conformation<sup>4,7</sup>. In the thermally-induced phase (Figure 2, d), two new peaks in the amide I region appear:  $1667\text{ cm}^{-1}$  and  $1682\text{ cm}^{-1}$ . While the first

peak, at  $1667\text{ cm}^{-1}$  shows tendency to  $\beta$ -turn secondary structure<sup>4,7</sup> the  $1682\text{ cm}^{-1}$  can be assigned to antiparallel  $\beta$ -sheet conformation<sup>7,8,11</sup>.

FTIR spectrum of the native FFF nanospheres shows a single wide peak at  $1661\text{ cm}^{-1}$  (Figure 2, e). This peak was already mentioned above as indicator of  $\beta$ -turn. FFF-fiber-like morphology observed after thermally induced phase transition is described by completely different FTIR spectral signature (Figure 2). The FTIR peak at  $1661\text{ cm}^{-1}$ , found in the native FFF-phase disappears and three new peaks at  $1634\text{ cm}^{-1}$ ,  $1650\text{ cm}^{-1}$  and  $1670\text{ cm}^{-1}$  are observed, indicating full refolding into new peptide organization. The first peak, at  $1634\text{ cm}^{-1}$  is a well-known fingerprint of antiparallel  $\beta$ -sheet secondary structure, and can be associated with  $\beta$ -sheet arrangement<sup>12</sup>. The second peak, at  $1650\text{ cm}^{-1}$  is assigned to aperiodic secondary structures involving type I, II, Via' and VII  $\beta$ -turns<sup>5</sup>, and the third peak, located at  $1670\text{ cm}^{-1}$  can be also related to  $\beta$ -turn<sup>4,7,8</sup>.

The aforementioned changes in the FTIR peaks' location in the amide I region for FF, LL and FFF nanostructures demonstrate that phase transition process occurring at elevated temperature might induce deep conformational transition from  $\beta$ -turn to  $\beta$ -sheet secondary structure. It is interesting to note that thermal treatment of the amyloid  $\beta$ -peptide, which contains the FF peptide, could also lead to secondary structure transition (from  $\alpha$ -helix to  $\beta$ -sheet), with the appearance of a new peak<sup>13</sup> at  $1634\text{ cm}^{-1}$ .

In contrast to the found thermally induced  $\beta$ -turn to  $\beta$ -sheet transition in FF, LL and FFF nanostructures, originally Cyc-FF have steady FTIR spectra at any temperature upto  $180^\circ\text{C}$  (Figure 2 g and Figure 2 h). This indicates that the secondary structure of original Cyc-FF PNF does not change with temperature. In both phases (before and after heating at  $180^\circ\text{C}$ ), a large single peak at  $1674\text{ cm}^{-1}$  accompanied with a few small peaks

are recorded (Figure 2, g and Figure 2, h). This stable FTIR frequency spectrum can be related to  $\beta$ -turn secondary structure<sup>7,8</sup>, which means that Cyc-FF PNF do not adopt  $\beta$ -sheet conformation when they are thermally heated to 180°C.

Thus native nanostructures of FF-, LL- and FFF- peptides subjected to thermally induced phase transition demonstrate similar tendency of deep modification of their FTIR spectra when new fibrillar phase has absolutely different FTIR frequency structure compared to the native one which is the evidence of refolding the original peptide secondary structures. Analysis of these spectra allows to define that induced fiber phase of aforementioned structures can be ascribed to  $\beta$ -sheet folding. Self-assembled original Cyclic-FF demonstrates surprising temperature stable FTIR spectra. These conclusions are completely consistent with morphological and CD data.

### **3. Electronic Density of States calculation of FFF dimer**

To check the effect of inter molecule interaction we have calculated with the VASP Density Functional Theory (DFT) code, the dimer binding energy and electronic structure for an anti-parallel hydrogen bonded dimer and a  $\pi$  stacked dimer. As described in the methods part (copied here for convenience): DFT calculations were carried out with the Vienna Ab initio Simulation Package (VASP)<sup>13</sup> code with Perdew-Burke-Ernzerhof (PBE<sup>14</sup>) and Heyd-Scuseria-Ernzerhof (HSE06)<sup>15</sup> functionals with Van-der-Waals (VdW) correction<sup>16</sup>. We have used projector augmented wave (PAW)<sup>17</sup> pseudopotentials, energy cutoff of 800eV, gamma-point only calculation and a unit cell of 20x20x20 Å. The unit cell was built to allow enough vacuum between dimers so we can ignore cell replicas. We relaxed the structures until the forces were lower than 0.02 eV/Å. The

hydrogen bond stabilization energy is significant and is about  $\sim 0.2\text{eV}$  per bond ( $\sim 1\text{eV}$  per FFF dimer), when PBE+VdW functional is used. This total energy lowering is compared to that of the isolated monomer and is probably much smaller if compared to monomers in a polar solvent. However, it is related to the energy barrier for breaking the dimer and indicates stabilization of the dimer by the hydrogen bonds. The hydrogen bonded dimer showed little band gap reduction ( $\sim 0.1\text{eV}$ ) while the  $\pi$  stacked dimer showed around  $0.5\text{eV}$  band gap reduction which can be considered as significant. This is shown by the Density of States of those configurations shown in Figure 3 below:

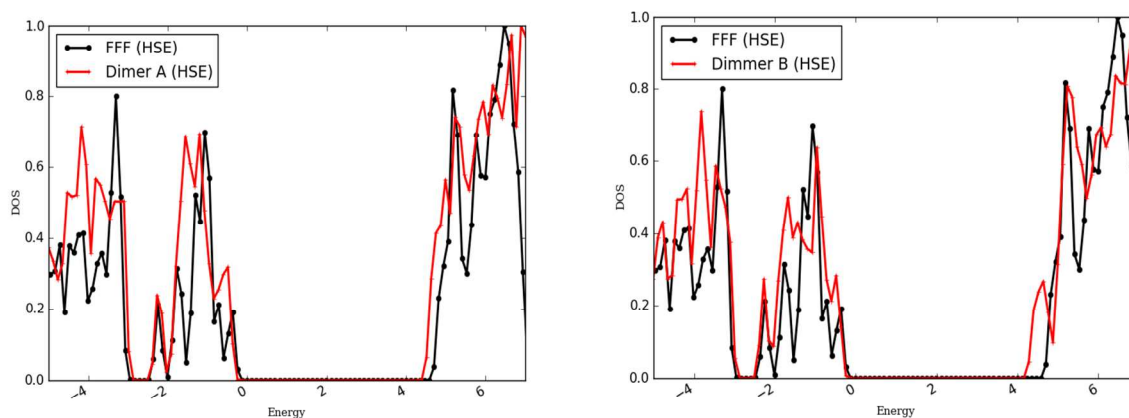


**Figure 3.** Left – HSE06 functional DOS of single FFF monomer (solid black), and a hydrogen bonded dimer (solid red). Right – HSE06 functional DOS of a single FFF monomer (solid black) and a dimer (solid red).

## References

- 
- <sup>1</sup> Ranjbar, B. & Gill, P. Circular Dichroism Techniques: Biomolecular and Nanostructural Analyses- A Review. *Chemical Biology & Drug Design* . **2009**, 74, 101.
- <sup>2</sup> B. Stuart, Biological Applications of Infrared Spectroscopy, Wiley, Chichester, 1997
- <sup>3</sup> Reches M.; Gazit E. Self-Assembly of Peptide Nanotubes and Amyloid-Like Structures by Charged-Termini-Capped Diphenylalanine Peptide Analogues. *Isr. J. Chem.* **2005**, 45, 363–371
- <sup>4</sup> Kong J.; Yu S. Fourier Transform Infrared Spectroscopic Analysis of Protein Secondary Structures. *Acta Biochim. Biophys. Sin. (Shanghai)*. 2007, 39(8), 549-59
- <sup>5</sup> Han T. H.; Ok T.; Kim J.; Shin D.O.; Ihee H.; Lee H. S., Kim S. O. Bionanosphere Lithography Via Hierarchical Peptide Self-Assembly of Aromatic Triphenylalanine. *Small*, 2010, 6, 945-951
- <sup>6</sup> Ryu J.; Park C. B. High Stability of Self-Assembled Peptide Nanowires Against Thermal, Chemical, and Proteolytic Attacks. *Biotechnol. Bioeng.* 2010, 105: 221–230.
- <sup>7</sup> Goormaghtigh E.; Cabiaux V.; Ruysschaert J.M. Secondary Structure and Dosage of Soluble and Membrane Proteins by Attenuated Total Reflection Fourier-Transform Infrared Spectroscopy on Hydrated Films. *Eur J Biochem.* 1990, 193(2), 409-20
- <sup>8</sup> Adochitei A.; Drochioiu G. Rapid Characterization of Peptide Secondary Structure by FT-IR Spectroscopy, *Rev. Roum. Chim.* 2011, 56, 783–791.
- <sup>9</sup> Reches M.; Gazit E. Designed Aromatic Homo-Dipeptides: Formation of Ordered Nanostructures and Potential Nanotechnological Applications. *Phys. Biol.* 2006, 3, 10-19
- <sup>10</sup> Barth A.; Zscherp C. What Vibrations Tell Us About Proteins, *Q Rev Biophys.* 2002, 35(4), 369-430.
- <sup>11</sup> Ma C.Y.; Rout M.K.; Mock W.Y.. Study of Oat Globulin Conformation by Fourier Transform Infrared Spectroscopy, *J. Agric Food Chem.*, 2001, 49(7), 3328-34.
- <sup>12</sup> Hamley I. W. Peptide Fibrillization. *Angew. Chem. Int. Ed.* 2007, 46, 8128-8147
- <sup>13</sup> Kresse, G.; Furthmüller, J. Efficient iterative schemes for ab initio total-energy calculations using a plane-wave basis set. *Phys. Rev. B* **1996**, 54, 11169–11186.
- <sup>14</sup> Perdew, J. P.; Burke, K.; Ernzerhof, M. Generalized gradient approximation made simple. *Phys. Rev. Lett.* **1996**, 77, 3865-73.
- <sup>15</sup> Krukau, A. V.; Vydrov, O. A.; Izmaylov, A. F.; Scuseria, G. E. Influence of the exchange screening parameter on the performance of screened hybrid functionals. *J. Chem. Phys.* **2006**, 125, 224106-12
- <sup>16</sup> Tkatchenko, A.; Scheffler, M. Accurate Molecular Van Der Waals Interactions from Ground-State Electron Density and Free-Atom Reference Data. *Phys. Rev. Lett.* **2009**, 102, 073005-12.
- <sup>17</sup> Blochl, P. E. Projector augmented-wave method. *Phys. Rev. B*, **1994**, 50, 17953-61. Kresse, G.; Joubert, D. From ultrasoft pseudopotentials to the projector augmented-wave method. *Phys. Rev. B*. **1999**, 59, 1758-66.